# Colloidal transport in twisted lattices of optical tweezers

Nico C. X. Stuhlmüller [1], Thomas M. Fischer [2], and Daniel de las Heras [1,*]

[1]*Theoretische Physik II, Physikalisches Institut, Universität Bayreuth, D-95440 Bayreuth, Germany*
[2]*Experimatalphysik X, Physikalisches Institut, Universität Bayreuth, D-95440 Bayreuth, Germany*

We simulate the transport of colloidal particles driven by a static and homogeneous drift force, and subject to the optical potential created by two lattices of optical tweezers. The lattices of optical tweezers are parallel to each other, shifted, and rotated by a twist angle. Due to a negative interference between the potential of the two lattices, flat channels appear in the total optical potential. At specific twist angles, known as magic angles, the flat channels percolate the entire system and the colloidal particles can then be transported using a weak external drift force. We characterize the transport in both square and hexagonal lattices of twisted optical tweezers.

I. INTRODUCTION

Optical tweezers [1] use optical gradient forces to manipulate micrometer-sized colloidal particles. Lattices of optical tweezers arranged in arbitrary patterns can be created, e.g., using diffractive optical elements [2], combining beam splitters and refractive optics [3], by means of computer-generated holograms [4], and even rapidly moving a single beam among different locations such that the desired pattern emerges as a result of a time-averaged optical potential [5–7].

Periodic lattices of optical tweezers in combination with a driving force are widely used to sort particles [8–11]. Using a three-dimensional periodic optical lattice, MacDonald *et al.* [8] were able to sort particles exploiting the differences in the interactions between the particles and the optical lattice. Also, as shown by Lacasta *et al.* [10], particles moving in a periodic optical potential can behave differently according to their size or particle index of refraction.

Motivated by the emerging field of twistronics [12], we adapt here the setup of Lacasta *et al.* [10] to model two sets of periodic lattices of optical tweezers that are parallel to each other and are also twisted by a given twist angle. Using computer simulations we study the transport of colloidal particles subject to the combined potential of both lattices and driven by a uniform and time-independent drift force. At specific twist angles, known as magic angles, the transport is more efficient due to the formation of flat channels in the combined optical potential of both lattices. Emergent phenomena in twisted bilayers, such as the occurrence of superconductivity in twisted graphene [13], has been observed in fundamentally different physical systems, including the appearance of quasi-one-dimensional channels along which Abrikosov vortices can freely flow in twisted pinning lattices [14], the formation of flat bands in twisted acoustic metamaterials [15], and enhanced colloidal transport in twisted magnetic patterns [16]. In contrast to single magnetic patterns, the magnetic potential of two twisted patterns develops flat channels along which it is possible to transport a magnetic colloidal particle applying

a weak drift force [16]. The flat channels percolate the entire system only for specific values of the twist angle. We show here with computer simulations that similar phenomena arise also in a fundamentally different system made of twisted lattices of optical tweezers.

II. MODEL AND RESULTS

A schematic of the model is shown in Fig. 1. The colloidal particles, which are driven by a drift force, are restricted to move in the middle plane between two parallel lattices of optical tweezers. We consider two periodic lattices of optical tweezers with square and hexagonal symmetries. The lattices are twisted by an angle α and shifted by half a unit lattice vector. A destructive interference between the optical potential generated by both lattices results in the formation of channels along which the potential is almost flat. Using a weak drift force it is then possible to transport the colloidal particles along the flat channels. At specific twist angles, known as magic angles, the flat channels percolate the entire system allowing transport over arbitrarily long distances.

A. Optical potential

Following Lacasta *et al.* [10], we approximate the optical potential at position $\mathbf{r}$ by

$$V(\mathbf{r}) = -\frac{V_0}{1 + e^{-A[g(\mathbf{r})-1]}}, \tag{1}$$

with positive constants A and V_0 that control the steepness and the depth of the optical potential, respectively. The spatial modulation and the interference between the two arrays of optical tweezers is controlled by the function

$$g(\mathbf{r}) = \sum_{i=1}^{N} \left\{ \cos\left[\mathbf{q}_i \cdot \left(\boldsymbol{R}_{-\alpha/2} \cdot \mathbf{r} - \frac{\mathbf{a}_1}{2}\right)\right] + \cos\left(\mathbf{q}_i \cdot \boldsymbol{R}_{\alpha/2} \cdot \mathbf{r}\right) \right\}, \tag{2}$$

where each of the two terms in the summation represents one of the lattices of optical tweezers.

─────────
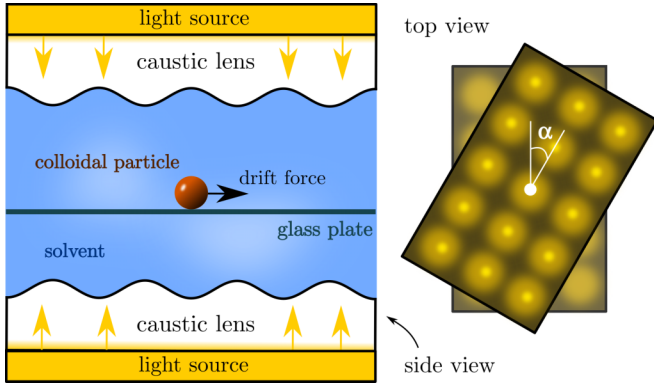*www.danieldelasheras.com; delasheras.daniel@gmail.com

FIG. 1. Schematic of the model: side (left) and top (right) views. A colloidal particle immersed in a solvent is located above a glass plate in the middle plane between two lattices of optical tweezers. The lattices are identical but are rotated by an angle α around an axis normal to them. The interference between the optical potential of both lattices creates an anisotropic potential landscape for the colloidal particles.

The lattices are shifted relative to each other by half of the first lattice vector of the single lattice prior to being rotated, $\mathbf{a}_1/2$, which we set along the x axis, i.e., $\mathbf{a}_1 = a\hat{\mathbf{e}}_x$, with a the magnitude of all the lattice vectors. The relative shift by half of a lattice vector maximizes the destructive interference between the two lattices at the flat channels. The matrix $\boldsymbol{R}_\theta$ is a rotation matrix by an angle θ around the axis normal to the lattice that passes through the origin. In Eq. (2) we rotate each lattice by an angle $\alpha/2$ in opposite directions such that

the total rotation between the lattices is the twist angle α. The reciprocal lattice vectors $\mathbf{q}_i$ are given by

$$\mathbf{q}_i = q \begin{pmatrix} \sin(\pi i/N) \\ \cos(\pi i/N) \end{pmatrix}, \tag{3}$$

where in the square lattice $N = 2$ and $q = 2\pi/a$, and in the hexagonal lattice $N = 3$ and $q = 2\pi/[a \sin(\pi/3)]$.

B. Magic angles

The total optical potential that results from the interference between both lattices is a moiré pattern. For specific twist angles the resulting potential is periodic. Among those angles for which the potential is periodic, we find the so-known magic angles, with particularly small lattice constants, given by [16]

$$\alpha_m(k, N) = 2 \arctan \left(\frac{\frac{1}{Nk+1} \sin\left(\frac{\pi}{N}\right)}{1 + \frac{1}{Nk+1} \cos\left(\frac{\pi}{N}\right)} \right), \tag{4}$$

where k is a natural number and again $N = 2$ for the square lattices and $N = 3$ for the hexagonal lattices.

The optical potential of lattices twisted at magic angles [see Figs. 2(a) and 2(b)] develops super unit cells of length given by approximately $a/[2 \sin(\alpha_m/2)]$. That is, the super unit cells grow by decreasing the magic angle. The super unit cells contain regions where the interference between the lattices is positive and hence the potential resembles that created by a single lattice, shown also as insets in Figs. 2(a) and 2(b). In addition, the super unit cells also contain regions at which the interference is mostly destructive. There, the potential develops flat channels along which transport is possible using
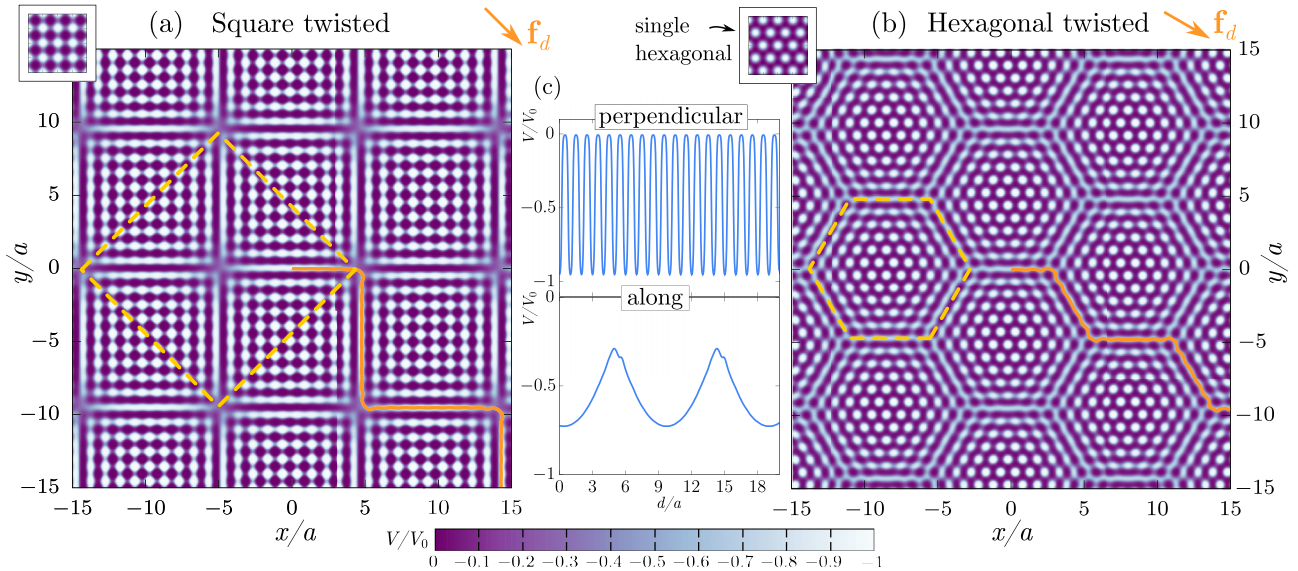

FIG. 2. Optical potential ($A = 1$) generated by two square (a) and two hexagonal (b) twisted lattices of optical tweezers twisted at magic angles: $\alpha_m \approx 6.026°$ in (a) and $\alpha_m \approx 6.009°$ in (b). A super unit cell of the moiré pattern is highlighted (yellow dashed line). A drift force $\mathbf{f}_d$ points in the direction of two consecutive flat channels (orange arrows) and drives the motion of the particles. Characteristic particle trajectories are depicted in orange. The amplitude of the external force is set to $f_d = 0.4V_0/a$ (a) and to $f_d = 0.8V_0/a$ (b). The optical potential of single square and hexagonal lattices is shown in the top left-hand corner of the panels. Cuts of the potential (square lattices) perpendicular and along the flat channel that passes through the origin are depicted in (c) as a function of the distance traveled by a particle initially at the origin. The force required to travel along the channel (negative gradient of the potential) is significantly smaller than the force required to travel perpendicular to the channel.
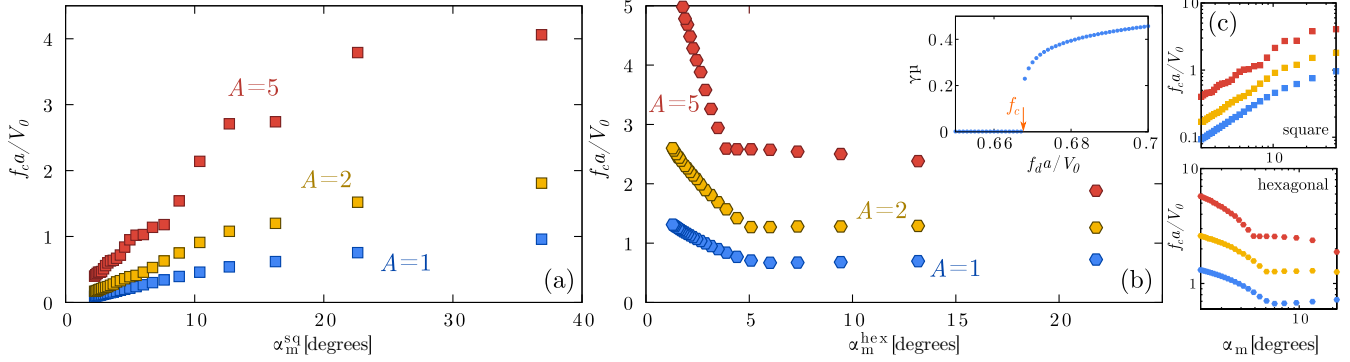
FIG. 3. Critical force in twisted square (a) and hexagonal (b) lattices as a function of the magic angle for different values of A. (c) shows the corresponding log‑log plots for both types of lattices, as indicated. A linear fit on the log‑log data for small magic angles returns a slope $s \approx 1$ in square lattices. In hexagonal lattices, $s \approx 1/3$ for both $A = 1$ and $A = 2$, and $s \approx 1/2$ for $A = 5$. The inset in (b) depicts the mobility μ vs the magnitude of the drift force f_d for the optical potential depicted in Fig. 2(a). The orange arrow indicates the value of the critical force f_c.

a weak drift force. The flat channels cross the super unit cell in square twisted lattices [Fig. 2(a)] and are located at the edges of the super unit cells in hexagonal twisted lattices [Fig. 2(b)]. We show in Fig. 2(c) a cut of the optical potential in the directions perpendicular to a flat channel and also along the flat channel, as indicated. The force required to travel along the flat channel (given by the negative gradient of the optical potential) is significantly weaker than that required to travel perpendicular to the flat channel. Increasing the parameter A makes the potential flatter along the central region of a flat channel. However, it also makes the potential steeper near the intersections between two flat channels. At the magic angles the flat channels percolate the entire system.

C. Computer simulations

We neglect inertial effects and therefore use overdamped dynamics to simulate the motion of a single colloidal particle. At high laser intensity the Brownian forces can be neglected as compared to the optical forces, we therefore set the temperature to zero such that Brownian motion does not hinder the phenomenology. The equation of motion for a single particle reads

$$\gamma \dot{\mathbf{r}} = -\nabla V(\mathbf{r}) + \mathbf{f}_d, \qquad (5)$$

where γ is the friction coefficient against the implicit solvent, $\dot{\mathbf{r}}$ indicates the time derivative of the position vector, and $\mathbf{f}_d$ is a homogeneous external drift force. The magnitude of a lattice vector a, the energy parameter of the optical potential V_0, and the friction coefficient γ define our system of units. The intrinsic timescale is therefore $\tau = \gamma a^2 / V_0$. We integrate the equation of motion using an adaptive Heun-Euler scheme [17], setting the relative allowed error per time step to 10^{-2} and the absolute allowed error in the positions to $10^{-4}a$.

D. Drift force

To drive the colloidal motion we use a drift force $\mathbf{f}_d$ pointing along the bisector of the directions of two flat channels

[see Figs. 2(a) and 2(b)]. Hence,

$$\mathbf{f}_d = f_d \begin{pmatrix} \cos \alpha_d \\ \sin \alpha_d \end{pmatrix}, \qquad (6)$$

where the angle is $\alpha_d(k) = (-1)^k \pi/4$ in square lattices and $\alpha_d(k) = (-1)^k \pi/6$ in hexagonal lattices, and the index $k \in \mathbb{N}$ is the same as for the magic angles in Eq. (4). The prefactor $(-1)^k$ alternates the direction of the drift force between the first and the fourth quadrants, reflecting the fact that the flat channels that support transport alternate from one magic angle to the next one.

Figures 3(a) and 3(b) show the magnitude of the critical drift force f_c required to transport colloidal particles along the flat channels; log‑log plots are shown in Fig. 3(c). To calculate f_c we measure in the simulations the colloidal mobility μ under the influence of the drift force,

$$\mu = \frac{|\Delta \mathbf{r}(t_f)|}{t_f f_d}, \qquad (7)$$

where $\Delta \mathbf{r}(t_f)$ is the distance traveled by a particle during a total time $t_f = 3000\tau$ in twisted square lattices, and $t_f = 1000\tau$ in twisted hexagonal lattices. The colloidal mobility vanishes for weak drift forces, increases rapidly at the critical drift force f_c, and it saturates for strong drift forces [see an example in the inset of Fig. 3(b)].

In square lattices, the critical force at which transport along the channels is activated decreases monotonically by decreasing the magic angle [see Fig. 3(a)]. For small magic angles, the critical force scales linearly with the magic angle [see Fig. 3(c)]. In hexagonal lattices [Fig. 3(b)], the critical force presents two distinct regimes. First, for small magic angles, there is a rapid decrease of f_c by increasing the magic angle. In the second regime, depending on the steepness of the potential, the critical force either slightly increases [e.g., $A = 1$ in Fig. 3(b)] or it slightly decreases [e.g., $A = 5$ in Fig. 3(b)]. For both square and hexagonal lattices, increasing the steepness of the potential A also increases the magnitude of the critical drift force. Increasing A makes the potential flatter along the channels, but it also increases the steepness of the potential at the intersection between two flat channels
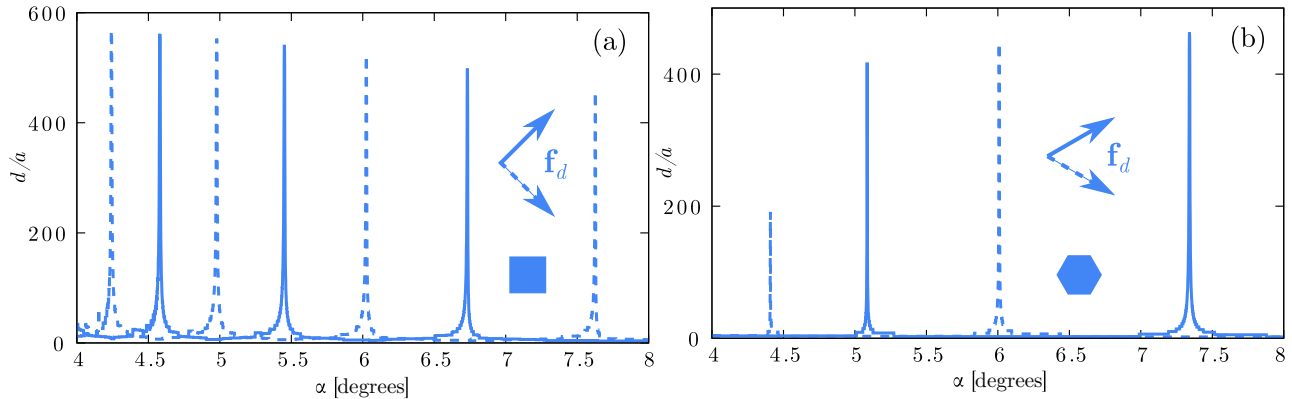
FIG. 4. Distance traveled by a particle originally at the origin in twisted square (a) and hexagonal (b) lattices ($A = 1$) as a function of the angle. In (a), the drift force $f_d = 0.4V_0/a$ acts for a total time $t = 3000$. The arrows indicate the direction of the drift force, rotated $45°$ (solid line) or $-45°$ (dashed line) with respect to the direction of the first lattice vector. In (b), $f_d = 0.8V_0/a$, $t = 1000\tau$, and the drift force is rotated $30°$ (solid line) or $-30°$ (dashed line) with respect to the direction of the first lattice vector.

which results in higher values of the magnitude of the critical force.

In Figs. 4(a) and 4(b) we represent the distance traveled by a particle, d, as a function of the twist angle for both square and hexagonal lattices, respectively. The particle is at time zero located at the axis of rotation of both lattices (i.e., in the middle of a flat channel). The motion is driven by a drift force acting for a total time 3000τ (1000τ) in square (hexagonal) lattices, and whose magnitude is larger than the critical force required to move particles at any of the magic angles that occur in the represented range of twist angles. For each lattice, we plot two curves, corresponding to drift forces that according to Eq. (6) point either in the first or in the fourth quadrant. The curves clearly show that the edges that support transport alternate from one magic angle to the next one. The distance traveled by the particles presents sharp peaks at the magic angles and hence even a small deviation from the magic angle has a marked effect on the transport. In square lattices the value of d at the magic angles decreases by increasing the magic angle since the critical force increases with the magic angle [see Fig. 3(a)], and we keep the magnitude of the drift force constant. The opposite behavior is observed in hexagonal lattices for the range of angles shown in Fig. 4(b). That is, d at the magic angles increases by increasing the magic angle. For the range of angles shown in Fig. 4(b), the critical drift force in hexagonal lattices decreases by increasing the magic angle, which explains the observed traveled distance at the magic angles.

III. CONCLUSIONS

Despite being substantially different systems, the colloidal transport in twisted optical lattices is quite similar to the transport in twisted magnetic patterns [16]. There, magnetic colloidal particles are located in the middle plane between two periodic magnetic patterns that are parallel to each other and are twisted by a given angle. A uniform external magnetic field $\mathbf{H}_{ext}$ normal to the patterns couples to the field created by both patterns $\mathbf{H}_p$. The total magnetic potential is then dominated by the cross term $V_{mag} \propto \mathbf{H}_{ext} \cdot \mathbf{H}_p$. Both the total magnetic potential in twisted patterns and the optical poten-

tial in twisted lattices of optical tweezers [Eq. (1)] coincide only in the limit $A \to 0$. Even though we have stayed away from that limit here, the transport in both systems shares similar characteristics, demonstrating the robustness of the phenomena.

The setup described here with optical lattices offers additional flexibility with respect to that in magnetic patterns. First, the steepness of the potential of single optical lattices, controlled here by the parameter A, can be adjusted experimentally by varying the width of the tweezers. Moreover, in contrast to magnetic patterns, optical tweezers are a standard experimental technique which is widely available and it can be used with nonmagnetic colloidal particles.

We have modeled the individual optical traps by isotropic potentials. Experimentally, it is possible to control the shape of the optical trap [18], and a certain degree of anisotropy is almost unavoidable. Above a certain threshold, the anisotropy of the optical trap can have an effect on, e.g., microrheology measurements [18], and might also alter the structure of the flat channels shown here. Controlling the anisotropy of the traps (e.g., the length-to-width aspect ratio and the direction of an elliptical trap) offers another degree of freedom to modify the colloidal transport.

Several types of external forces are available experimentally to drive the motion [19]. These include, among others, electric and magnetic fields, pressure gradients, and the gravitational field of Earth in the case of micron-sized colloidal particles with a substantial contrast between the bare and the solvent mass densities.

There exist other twist angles for which the combined potential of the two lattices is also periodic [16]. However, for those angles, the direction along which transport is possible along the flat channels changes inside the super unit cell. Hence, stronger drift forces are required to cause macroscopic transport.

We have focused here on the dilute regime where interparticle interactions do not play any role. Interesting collective effects appear in many-body particle systems driven on periodic landscapes, including structural transitions and directional locking [20–22]. It would be also interesting to study collective effects in the dynamics of many-body particles in

twisted lattices such as the superadiabatic forces [23,24] and the occurrence of solitons [25].

Another interesting extension of the present work is the characterization of the transport in twisted three-dimensional optical lattices. Moreover, using periodic two-dimensional magnetic patterns together with a homogeneous magnetic field, one can topologically transport magnetic colloidal particles placed above the patterns [26–28]. There exist special modulation loops of the orientation of the external field such that once the loop returns to its initial position the particle has been transported by one unit cell above the pattern. The

colloidal motion is topologically protected and takes place in a plane due to the two-dimensional nature of the magnetic patterns. Optical potentials could be used to extend the study of topologically protected colloidal transport to three-dimensional systems.

[1] A. Ashkin, J. M. Dziedzic, J. E. Bjorkholm, and S. Chu, Observation of a single-beam gradient force optical trap for dielectric particles, Opt. Lett. **11**, 288 (1986).

[2] E. R. Dufresne and D. G. Grier, Optical tweezer arrays and optical substrates created with diffractive optics, Rev. Sci. Instrum. **69**, 1974 (1998).

[3] E. Fällman and O. Axner, Design for fully steerable dual-trap optical tweezers, Appl. Opt. **36**, 2107 (1997).

[4] J. Liesener, M. Reicherter, T. Haist, and H. Tiziani, Multifunctional optical tweezers using computer-generated holograms, Opt. Commun. **185**, 77 (2000).

[5] K. Sasaki, M. Koshioka, H. Misawa, N. Kitamura, and H. Masuhara, Pattern formation and flow control of fine particles by laser-scanning micromanipulation, Opt. Lett. **16**, 1463 (1991).

[6] K. Visscher, S. Gross, and S. Block, Construction of multiple-beam optical traps with nanometer-resolution position sensing, IEEE J. Sel. Top. Quantum Electron. **2**, 1066 (1996).

[7] D. G. Grier, A revolution in optical manipulation, Nature (London) **424**, 810 (2003).

[8] M. P. MacDonald, G. C. Spalding, and K. Dholakia, Microfluidic sorting in an optical lattice, Nature (London) **426**, 421 (2003).

[9] P. T. Korda, M. B. Taylor, and D. G. Grier, Kinetically Locked-In Colloidal Transport in an Array of Optical Tweezers, Phys. Rev. Lett. **89**, 128301 (2002).

[10] A. M. Lacasta, J. M. Sancho, A. H. Romero, and K. Lindenberg, Sorting on Periodic Surfaces, Phys. Rev. Lett. **94**, 160601 (2005).

[11] A. Jonáš and P. Zemánek, Light at work: The use of optical forces for particle manipulation, sorting, and analysis, Electrophoresis **29**, 4813 (2008).

[12] S. Carr, D. Massatt, S. Fang, P. Cazeaux, M. Luskin, and E. Kaxiras, Twistronics: Manipulating the electronic properties of two-dimensional layered structures through their twist angle, Phys. Rev. B **95**, 075420 (2017).

[13] Y. Cao, V. Fatemi, S. Fang, K. Watanabe, T. Taniguchi, E. Kaxiras, and P. Jarillo-Herrero, Unconventional superconductivity in magic-angle graphene superlattices, Nature (London) **556**, 43 (2018).

[14] W. Li, C. J. O. Reichhardt, B. Jankó, and C. Reichhardt, Vortex dynamics, pinning, and angle-dependent motion on moiré patterns, Phys. Rev. B **104**, 024504 (2021).

[15] S. M. Gardezi, H. Pirie, S. Carr, W. Dorrell, and J. Hoffman, Simulating twistronics in acoustic metamaterials, 2D Mater. **8**, 031002 (2021).

[16] N. C. X. Stuhlmüller, T. M. Fischer, and D. de las Heras, Enhanced colloidal transport in twisted magnetic patterns, Commun. Phys. **5**, 48 (2022).

[17] F. Sammüller and M. Schmidt, Adaptive Brownian dynamics, J. Chem. Phys. **155**, 134107 (2021).

[18] A. B. Matheson, T. Mendonca, G. M. Gibson, P. A. Dalgarno, A. J. Wright, L. Paterson, and M. Tassieri, Microrheology with an anisotropic optical trap, Front. Phys. **9**, 621512 (2021).

[19] H. Löwen, Colloidal dispersions in external fields: recent developments, J. Phys.: Condens. Matter **20**, 404201 (2008).

[20] C. Reichhardt and C. J. Olson Reichhardt, Dynamical Ordering and Directional Locking for Particles Moving Over Quasicrystalline Substrates, Phys. Rev. Lett. **106**, 060603 (2011).

[21] C. Reichhardt and C. J. O. Reichhardt, Depinning and nonequilibrium dynamic phases of particle assemblies driven over random and ordered substrates: a review, Rep. Prog. Phys. **80**, 026501 (2017).

[22] C. Reichhardt and C. J. O. Reichhardt, Structural transitions and dynamical regimes for directional locking of vortices and colloids driven over periodic substrates, J. Phys.: Condens. Matter **24**, 225702 (2012).

[23] D. de las Heras and M. Schmidt, Flow and Structure in Nonequilibrium Brownian Many-Body Systems, Phys. Rev. Lett. **125**, 018001 (2020).

[24] M. Schmidt, Power functional theory for many-body dynamics, Rev. Mod. Phys. **94**, 015007 (2022).

[25] A. P. Antonov, A. Ryabov, and P. Maass, Solitons in overdamped Brownian dynamics, Phys. Rev. Lett. **129**, 080601 (2022).

[26] J. Loehr, M. Loenne, A. Ernst, D. de las Heras, and T. M. Fischer, Topological protection of multiparticle dissipative transport, Nat. Commun. **7**, 11745 (2016).

[27] D. de las Heras, J. Loehr, M. Loenne, and T. M. Fischer, Topologically protected colloidal transport above a square magnetic lattice, New J. Phys. **18**, 105009 (2016).

[28] J. Loehr, D. de las Heras, M. Loenne, J. Bugase, A. Jarosz, M. Urbaniak, F. Stobiecki, A. Tomita, R. Huhnstock, I. Koch, A. Ehresmann, D. Holzinger, and T. M. Fischer, Lattice symmetries and the topologically protected transport of colloidal particles, Soft Matter **13**, 5044 (2017).